Chemical Engineering Journal 403 (2021) 126395

Contents lists available at ScienceDirect

Chemical Engineering Journal

journal homepage: www.elsevier.com/locate/cej

N-coordinated Co containing porous carbon as catalyst with improved dispersity and stability to activate peroxymonosulfate for degradation of organic pollutants

Hongchao Li[a], Jieshu Qian[a,c,*], Bingcai Pan[b,c]

[a] Jiangsu Key Laboratory of Chemical Pollution Control and Resources Reuse, School of Environmental and Biological Engineering, Nanjing University of Science and Technology, 200 Xiao Ling Wei, Nanjing 210094, China
[b] State Key Laboratory of Pollution Control and Resource Reuse, School of the Environment, Nanjing University, Nanjing 210023, China
[c] Research Center for Environmental Nanotechnology (ReCENT), Nanjing University, Nanjing 210023, China

HIGHLIGHTS

- Co phthalocyanine as one of pyrolysis precursors for PMS activation catalyst.
- N coordination strongly binds Co and allows uniform distribution of Co species.
- The catalyst contains high Co content of 8.0 wt% yet low Co leaching of less than 50 μg/L.
- The PMS/catalyst system exhibits remarkable reactivity toward several pollutants.

GRAPHICAL ABSTRACT

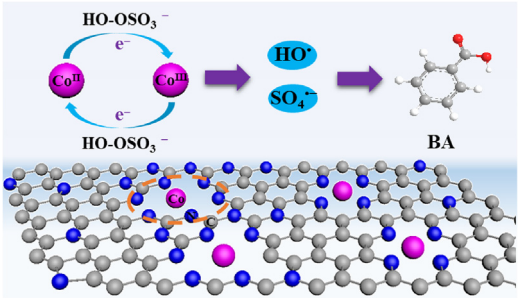

ARTICLE INFO

Keywords:
Advanced oxidation processes
Peroxymonosulfate
N coordination
Cobalt-based catalyst
Water decontamination

ABSTRACT

Co-based carbonaceous materials are among the most effective heterogeneous catalysts to activate peroxymonosulfate (PMS) for the degradation of organic pollutants in water. However, present examples normally suffer the aggregation of catalyst and/or the leakage of active Co species especially when the Co content is high, resulting in a loss of reactivity and potential environmental risk. In this study, we report the use of a mixture of Co phthalocyanine and melamine as precursor for the preparation of a carbonaceous catalyst with N-coordinated Co (Co-NG) for PMS activation. The presence of Co phthalocyanine in the precursor facilitates the uniform distribution of Co species in carbonaceous substrate with high Co content of 8.0 wt%, thus exhibiting remarkable catalytic reactivity for the degradation of a variety of organic pollutants. More importantly, the strong coordination by N atoms significantly enhances the Co stability and reduces the Co leaching during cyclic use. Experiment results demonstrate that both sulfate radicals ($SO_4^{\bullet -}$) and hydroxyl radicals ($HO^{\bullet}$) contribute to the pollutant degradation with $SO_4^{\bullet -}$ as the main reactive species. Other reaction parameters including solution pH, the presence of inorganic anions, and natural organic matters were also investigated and evaluated. We reckon this study provides new insights for the design of efficient Co-based carbonaceous catalysts with high Co stability for water treatment application.

* Corresponding author at: Jiangsu Key Laboratory of Chemical Pollution Control and Resources Reuse, School of Environmental and Biological Engineering, Nanjing University of Science and Technology, 200 Xiao Ling Wei, Nanjing 210094, China.
E-mail address: qianjieshu@njust.edu.cn (J. Qian).

https://doi.org/10.1016/j.cej.2020.126395
Received 29 May 2020; Received in revised form 20 July 2020; Accepted 21 July 2020
Available online 26 July 2020

1. Introduction

Advanced oxidation processes involving hydroxyl radicals ($HO^{\bullet}$) and/or sulfate radicals ($SO_4^{\bullet-}$) as the main reactive species have attracted tremendous attention for the oxidative degradation of refractory organic pollutants during the past decade [1]. Both species could be simultaneously generated from the decomposition of peroxymonosulfate (PMS) in response to external stimuli such as ultraviolet [2], ultrasound [3], microwave [4], electricity [5], chemicals [6], and especially the use of transition metals [7] as catalysts which is feasible and practical for scale-up application due to the easy-operation and low-cost. Among the commonly studied transition metals (M = Co, Fe, Mn, and Cu), Co is considered as the most effective candidate as its standard redox potential (1.82 V) is very close to that of PMS (1.75 V) [7]. However, the Co-based homogeneous catalytic oxidation process suffers potential environmental risk due to the toxicity of Co^{2+} [8]. Consequently, various heterogeneous Co-based catalysts such as Co oxides [9,10] and supported Co catalysts [11–15] have been developed for the activation of PMS, in the hope of mitigating the release of Co.

Graphitic carbon nitride (g-C_3N_4) possesses electron-rich six N-atoms cavities that could provide stable coordination environment for transition metals, and has thus been widely used as substrate for the preparation of heterogeneous catalysts (i.e., transition metal doped g-C_3N_4, M/g-C_3N_4) [16–20]. Moreover, the strong M−N interaction allows the distribution of metal species in highly dispersed forms such as nanocluster and even single atom, rendering high catalytic activity [18–20]. For examples, Wang *et al.* [19] reported that the concentration of Co in the solution released from Co/g-C_3N_4 is much lower than that from Co_3O_4. Xie *et al.* [20] reported that the catalytic activity of Co/g-C_3N_4 is ca. 7–13 times higher than Co_3O_4 for PMS activation. A generally adopted preparation method for Co/g-C_3N_4 is the pyrolysis of a mixture of N-containing precursors (i.e., urea, dicyandiamide, and melamine) and Co salts (i.e., $CoCl_2$ and $Co(NO_3)_2$) [19,20]. However, severe aggregation of g-C_3N_4 might occur during pyrolysis [17], which could significantly reduce the catalytic activity of the catalyst.

The composition of precursors could dictate the preformed structure before pyrolysis and is thus of great importance in the structural design of catalysts. Previous studies have demonstrated that the introduction of porous carbon materials (i.e., mesoporous carbon [21], graphene [22]) and natural carbohydrates (i.e., glucose [17]) into the precursors is an effective strategy to inhibit the aggregation of g-C_3N_4. We expect that the use of substituent Co precursor might also make similar contribution. Metal phthalocyanine is a conjugated macrocyclic complex containing M−N_4 structure as the active site. The pyrolysis of metal phthalocyanine yields porous carbonaceous matrix [23], which is expected to suppress the aggregation of g-C_3N_4. Meanwhile, the strong binding affinity with metal as well as the steric hindrance of the macrocyclic structure of phthalocyanine facilitate the dispersed distribution of metal species and effectively inhibit the unfavored formation of metal particles during pyrolysis [24]. With more virtues of high specific surface area and hierarchical porous structure, we postulate that the use of Co phthalocyanine as precursor could generate Co containing carbonaceous catalyst with much enhanced stability as well as reactivity for PMS activation.

In this study, we report the use of a mixture of Co phthalocyanine and melamine as precursor for the preparation of Co coordinated by N in graphite (Co-NG) catalyst with high Co content yet uniform distribution, via a convenient one-step pyrolysis. The morphology, crystalline structure, and chemical state of Co-NG as well as several comparative samples were characterized. The catalytic performance and mechanism of Co-NG towards the activation of PMS for the generation of $SO_4^{\bullet-}$ and $HO^{\bullet}$ were investigated by using benzoic acid (BA) as the target pollutant. In addition, the effects of several important parameters such as Co-NG dosage, PMS dosage, coexisting substrates (i.e., inorganic anions and natural organic matters), and solution pH on the removal of BA were examined. Moreover, the stability and reusability of Co-NG were investigated.

2. Material and methods

2.1. Materials

Co phthalocyanine was purchased from Tokyo Chemical Industry Co., Ltd. BA, ibuprofen (IBU), p-hydroxybenzoic acid (PHBA), bisphenol A (BPA), 4-chlorophenol (4-CP), 5,5-dimethyl-1-pyrroline-N-oxide (DMPO), methanol (MeOH), *tert*-butyl alcohol (TBA), hydrogen peroxide (H_2O_2), potassium peroxydisulfate (PDS), and potassium peroxymonosulfate (PMS, available as Oxone) were bought from Shanghai Aladdin Biochemical Technology Co., Ltd. Cobalt nitrate hexahydrate ($Co(NO_3)_2{\cdot}6H_2O$) and melamine were purchased from the Sinopharm Chemical Reagent Co., Ltd. Natural organic matters (NOM) from Suwannee River was supplied by International Humic Substances Society. Deionized water (18.2 MΩ/cm) was used in this study.

2.2. Preparation of catalyst

The Co coordinated by N in graphite (Co-NG) sample was synthesized according to a reported method with slight modification [25]. Typically, 0.23 g Co phthalocyanine and 4.0 g melamine were mixed and grinded for 30 min, and then the mixture was transferred to a ceramic crucible and calcinated in tube furnace under N_2 atmosphere at 600℃ for 2.0 h with a heating rate of 3.0 ℃/min. After cooling down to room temperature, the resulted powder was treated with 1.0 M H_2SO_4 at 80 ℃ to dissolve the residue Co particles, and then washed with DI water several times, and finally dried at 60 ℃ in air oven for next run. The obtained catalyst is referred to as Co-NG. For comparison, another Co doped g-C_3N_4 (denoted as Co-CN) sample was prepared by using Co $(NO_3)_2{\cdot}6H_2O$ (0.12 g) as Co precursor. In addition, g-C_3N_4 (CN) and N modified porous carbon (NG) samples were prepared by calcination melamine and the mixture of melamine (4.0 g) and phthalocyanine (0.21 g), respectively.

2.3. Catalytic reactions

The catalytic oxidation experiments were conducted in a 100 mL beaker containing 50 mL reaction solution under magnetic stirring at 20.0 ± 1 ℃. Typically, PMS (1.0 mM) and pollutants (i.e., BA, 50 μM) were added to the reactor to form homogeneous solution, followed by the addition of catalyst (20 mg/L) to the homogeneous solution to initiate the reaction. The solution pH during the reaction was monitored and adjusted by 0.05 M $HClO_4$ or NaOH, in order to keep the pH at the desired value with a fluctuation below 0.5. At predetermined reaction time, 1.5 mL solution was removed with a syringe, filtered with a 0.22 μm filter, and quenched immediately by excessive Na_2SO_3 prior to analysis. To evaluate the reusability, the used catalyst was collected vis centrifugation after each run, washed with DI water and ethanol for three times, respectively, and finally dried at 60 ℃ under vacuum. The recovered catalyst was used in the next run of batch experiment.

2.4. Characterizations and analytical methods

The specific surface area and pore structure of the catalysts were characterized by N_2 adsorption/desorption experiments performed on an automated gas sorption analyzer (Quantachrome Nova 3000). The morphologies of samples were observed by transmission electron microscope (TEM, FEI Tecnai G20) and high-resolution transmission electron microscope (HRTEM, FEI Tecnai G20). The crystal structures of the catalysts were recorded on an X-Ray diffractometer (XRD, ALR X'TRA). X-ray photoelectron spectroscopy (XPS, ESCALAB-2) was used for analyzing the chemical state of elements. All binding energies were corrected with respect to C 1 s peak at 284.6 eV. Fourier transform infrared (FT-IR) spectra were recorded on a Nicolet iS5 spectrometer

with an attenuated total reflectance (ATR) accessory. Electron paramagnetic resonance (EPR, EMX-10/12) spectrometry was employed to identify the generation of $SO_4^{\bullet -}$ and $HO^{\bullet}$ by using DMPO as the spin trapping agent. The total organic carbon (TOC) was measured by a TOC-V CPN analyzer. The Co content leached in solution was determined by inductively coupled plasma mass spectrometry (ICP-MS, NexION 300X). The concentration of organic pollutants was determined by high performance liquid chromatography (HPLC, UltiMate 3000) system. The degradation of BA followed a pseudo-first-order kinetics, as described by eq (1):

$$\ln[\frac{[BA]_t}{[BA]_0}] = -kt \quad (1)$$

where $[BA]_t$ and $[BA]_0$ represent the concentration of BA at the time of t and 0, respectively. k is the apparent rate constant for the degradation of BA. The degradation intermediates of BA were identified by high performance liquid chromatography-mass spectrum (LC-MS, Q Exactive Focus) and gas chromatography-mass spectrum (GC–MS, TRACE1310/ISQ LT). Detailed experiment conditions were shown in our previous studies [16,26].

3. Results and discussion

3.1. Characterization of the catalysts

The basic properties of the CN, Co-CN, NG, and Co-NG samples are summarized in Table 1. During the pyrolysis, the decomposition of phthalocyanine is accompanied by the release of gases (i.e., H_2O, CO, and CO_2.) [27], which facilitates higher porosity (see the specific surface area of NG and CN in Table 1, 151.1 versus 5.2 m^2/g). Consequently, the obtained Co-NG catalyst possesses much higher specific surface area (132.6 m^2/g) than Co-CN (35.6 m^2/g). Moreover, the Co-NG sample exhibits much higher Co content than Co-CN (8.0 versus 1.6 wt%, Table 1).

The morphologies of the four samples, i.e. CN, Co-CN, NG, and Co-NG, were investigated by TEM and HRTEM. Representative TEM images in Fig. 1a-d show that all samples exhibit irregular particle structure. The HRTEM image in Fig. 1e and selected area electron diffraction (SAED) pattern in Fig. 1f of the Co-NG sample show that Co nanoparticles could not be detected. The elemental mappings images showing the distribution of C (Fig. 1g), N (Fig. 1h), and Co (Fig. 1i) elements suggest that the Co species are highly dispersed in the substrate. Here we would like to comment that it is interesting to see the absence of apparent Co particles in Co-NG with such high Co content (8.0 wt%), which must be due to the unique structural features of the substrate.

The ATR-FT-IR spectra of the four samples are shown in Fig. 2a, from which one could see the broad band at 3400–2800 cm^{-1}, ascribing to the N–H stretching vibration of g-C_3N_4 [28], of both CN and Co-CN samples. Meanwhile, the strong absorption band from 1700 to 1000 cm^{-1} and the intense peak at 809 cm^{-1} are assigned to the skeletal stretching and breathing mode of the tris-s-triazine units, respectively [29]. With respect to the NG and Co-NG samples, the characteristic peaks of typical g-C_3N_4 become obscure. We hypothesize that this is probably due to the formation of carbon matrix in the pyrolysis of Co phthalocyanine, which could greatly suppress the polymerization of melamine.

Table 1
Basic properties of the obtained catalysts.

Materials	CN	NG	Co-CN	Co-NG
Co loading, wt. %	0	0	1.6	8.0
Surface area, m^2/g	5.2	151.1	35.6	132.6
Average pore size , nm	19.4	8.2	20.9	9.2
Pore volume, cm^3/g	0.025	0.311	0.183	0.272

The XRD patterns of the four samples are presented in Fig. 2b. The diffraction patterns of both CN and Co-CN samples match well with the g-C_3N_4. The diffraction peaks at 13.0° and 27.4°, corresponding to the (1 0 0) and (0 0 2) facets, are attributed to the periodic in-plane tri-s-triazine units and the inter-layer stacking of aromatic systems, respectively [29]. Interestingly, the peaks of the (0 0 2) facets of g-C_3N_4 in the NG and Co-NG samples shift slightly to lower angle with much weakened intensities, suggesting the destruction of the crystallinity of g-C_3N_4 due to the introduction of Co phthalocyanine into the precursor. Moreover, the characteristic peaks of Co species could not be observed in Co-CN sample and especially Co-NG sample with much higher Co content, indicating the absence of crystalline Co species and the highly dispersive distribution of Co atoms.

The chemical compositions and elemental states of Co-CN and Co-NG were further analyzed by XPS measurement. The XPS survey spectra are presented in Fig. 2c, from which one sees the characteristic peaks of C, N, O, and Co elements. The deconvolutions of the XPS C 1 s, N 1 s, and Co 2p spectra of both samples are presented in Fig. 2d, 2e, and 2f, respectively. Fig. 2d shows that the C 1 s peak of Co-CN could be deconvoluted to be three peaks at 284.6, 285.9, and 287.8 eV, corresponding to the sp^2 hybridized C in C = C, C-OH, and N-C = N [30]. While for C 1 s peak of Co-NG, the deconvolution generates three peaks at 284.6, 286.1, and 287.9 eV, ascribing to the C = C, C-N&C-OH, and C = N&C = O [31]. The significantly enhanced intensity of the peak at 284.6 eV (C = C) of Co-NG than Co-CN might suggest a higher degree of carbonization due to the introduction of Co phthalocyanine in precursor. Fig. 2e shows that N 1 s peak of Co-CN is deconvoluted to be two peaks at 398.2 and 399.6 eV, corresponding to the sp^2-hybridized N in triazine rings (C-N = C) and the tertiary nitrogen N-$(C)_3$&C-NH-C groups [16]. While for N 1 s peak of Co-NG, the deconvolution generates three peaks at 398.0, 398.8 and 400.2 eV, assigning to pyridinic, pyrrolic and graphitic N species [31]. Fig. 2f shows that the Co 2p peaks of both samples could be deconvoluted to be two main peaks at 781.6 and 796.8 eV, attributing to Co $2p_{3/2}$ and Co $2p_{1/2}$, respectively. The peak intensity in Co-CN is much weaker than that of Co-NG due to the lower Co content in Co-CN. The sharp peak at 781.6 eV in Co $2p_{3/2}$ of Co-NG could be attributed to Co-N bond, similar to Co phthalocyanine and Co-N-C catalysts reported previously [19,32,33].

3.2. Catalytic performance of Co-NG.

The catalytic performances of the four samples for the activation of PMS are shown in Fig. 3a, represented by the degradation of target molecule BA versus time. One sees that negligible abatement of BA is observed when PMS is used alone. The use of CN and NG as catalysts results in only less than 8% BA removal in 15 min. With respect to the use of two Co containing catalysts, 40% BA degradation is observed in PMS/Co-CN system, while nearly 100% BA degradation is achieved in PMS/Co-NG system. The catalytic performance of Co-NG is much higher than that of Co-based oxide in terms of the oxidative removal of BA [34]. The data of BA degradation using PMS/Co-NG and PMS/Co-CN systems are fitted to pseudo-first-order kinetics, as shown in Fig. S1. The apparent rate constant in PMS/Co-NG system is calculated to be 0.390 min^{-1}, which is about 13 times of that in PMS/Co-CN system (0.030 min^{-1}). The superior catalytic performance of Co-NG to Co-CN could be attributed to both effects of the larger specific surface area and higher Co loading.

In addition, IBU, PHBA, BPA, and 4-CP were also completely degraded by PMS/Co-NG within 15 min in the rate order of 4-CP > PHBA > BPA > IBU, as shown in Fig. 3b. This nonselective and excellent catalytic oxidation performance suggests that PMS/Co-NG could be employed for the degradation of a variety of refractory organic pollutants. The catalytic activity of Co-NG towards other oxidants (i.e., H_2O_2 and PDS) were further examined. As shown in Fig. S2, less than 6% BA is degraded in H_2O_2/Co-NG and PDS/Co-NG systems,

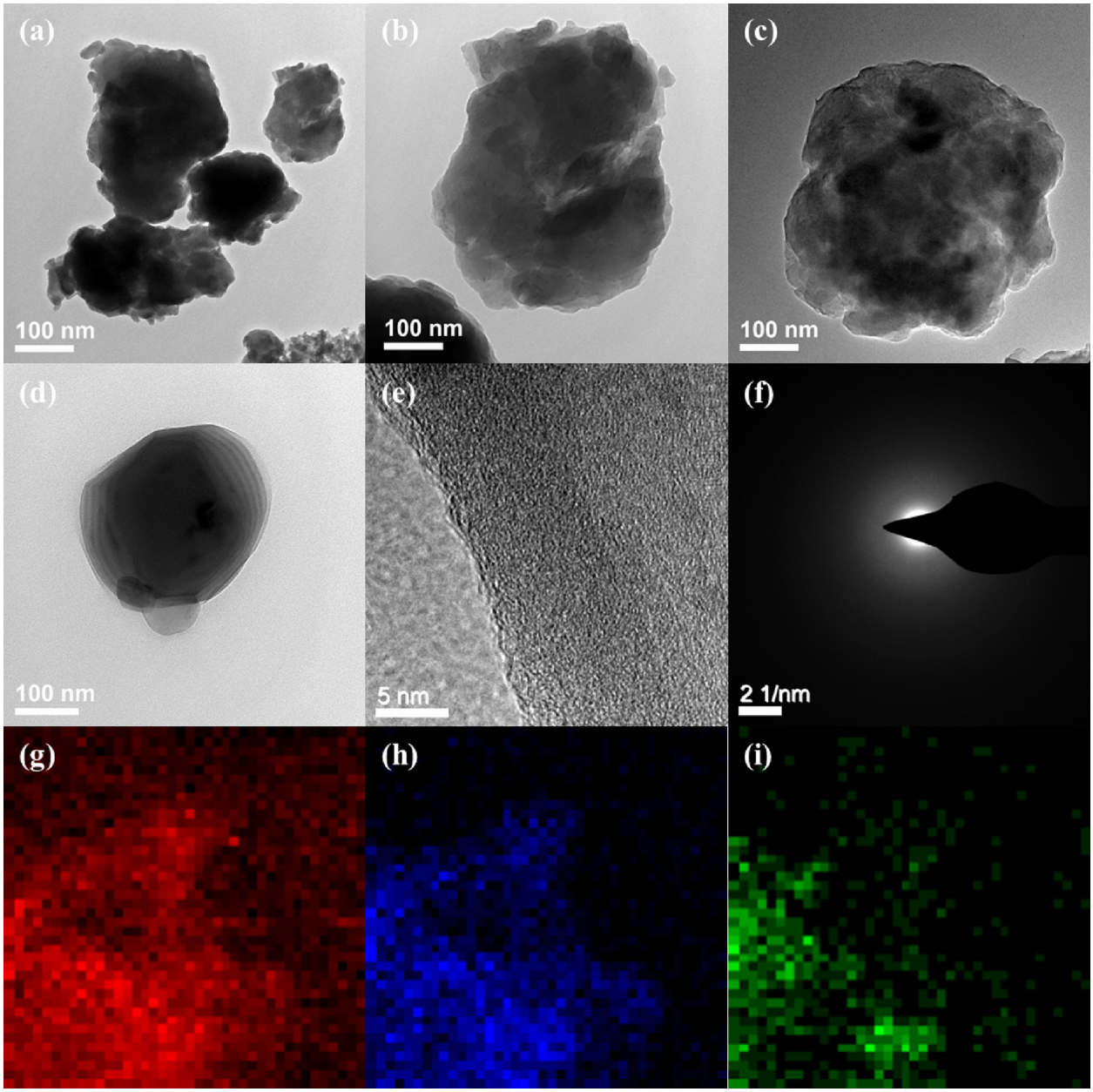

Fig. 1. Representative TEM images of (a) CN, (b) Co-CN, (c) NG, and (d) Co-NG. (e) High-resolution TEM image and (f) SAED patterns of Co-NG. Elemental mappings of (g) C, (h) N, and (i) Co elements of Co-NG.

suggesting the inferior catalytic ability of Co-NG towards H_2O_2 and PDS compared to PMS. This is probably because the peroxy bond (O-O) in PMS is more susceptible to cleavage than other two peroxides due to the asymmetric structure of PMS [1].

3.3. Mechanism of BA degradation

To explore the degradation mechanism of BA in PMS/Co-NG system, radical quenching experiments were conducted by using both MeOH and TBA as radical scavengers. MeOH is considered to be an efficient quenching reagent for both $HO^{\bullet}$ and $SO_4^{\bullet-}$ with second-order rate constant of 9.7×10^8 and 3.2×10^6 $M^{-1}s^{-1}$ [35,36], respectively. Fig. 4a shows that only 13% BA is removed after the addition of 0.1 M MeOH, suggesting $HO^{\bullet}$ and/or $SO_4^{\bullet-}$ are the major reactive species for the degradation of BA. With respect to the use of TBA, the reaction rates with $HO^{\bullet}$ and $SO_4^{\bullet-}$ are 3.8×10^8 and 7.6×10^5 $M^{-1}s^{-1}$ [35,36], thus it is effective for identifying the contribution of each species for the remove of BA. Fig. 4a shows that about 79% BA is removed in the presence of 0.1 M TBA. These results demonstrate that the TBA is not effective in inhibiting the BA degradation and imply that $SO_4^{\bullet-}$ is a major contributor and $HO^{\bullet}$ is a minor contributor for the degradation of BA.

EPR studies were employed to further confirm the reactive species involved in different systems by employing DMPO as trapping agent. In Fig. 4b, one could hardly observe the characteristic signals of both $HO^{\bullet}$ and $SO_4^{\bullet-}$ adducts in PMS alone, PMS/CN, and PMS/NG systems, suggesting that negligible amounts of $HO^{\bullet}$ and $SO_4^{\bullet-}$ are generated in those systems. With respect to the PMS/Co-CN and PMS/Co-NG systems, characteristic signals of 5,5-dimethyl-1-pyrrolidone-2-oxyl (DMPOX) with peak intensity of 1:2:1:2:1:2:1 are evident. Previous study has suggested that the formation of DMPOX could be due to the oxidation of DMPO via either radical or nonradical pathway [37]. In combination with the results described in the previous paragraph, we postulate that $HO^{\bullet}$ and $SO_4^{\bullet-}$ are the reactive species for the formation

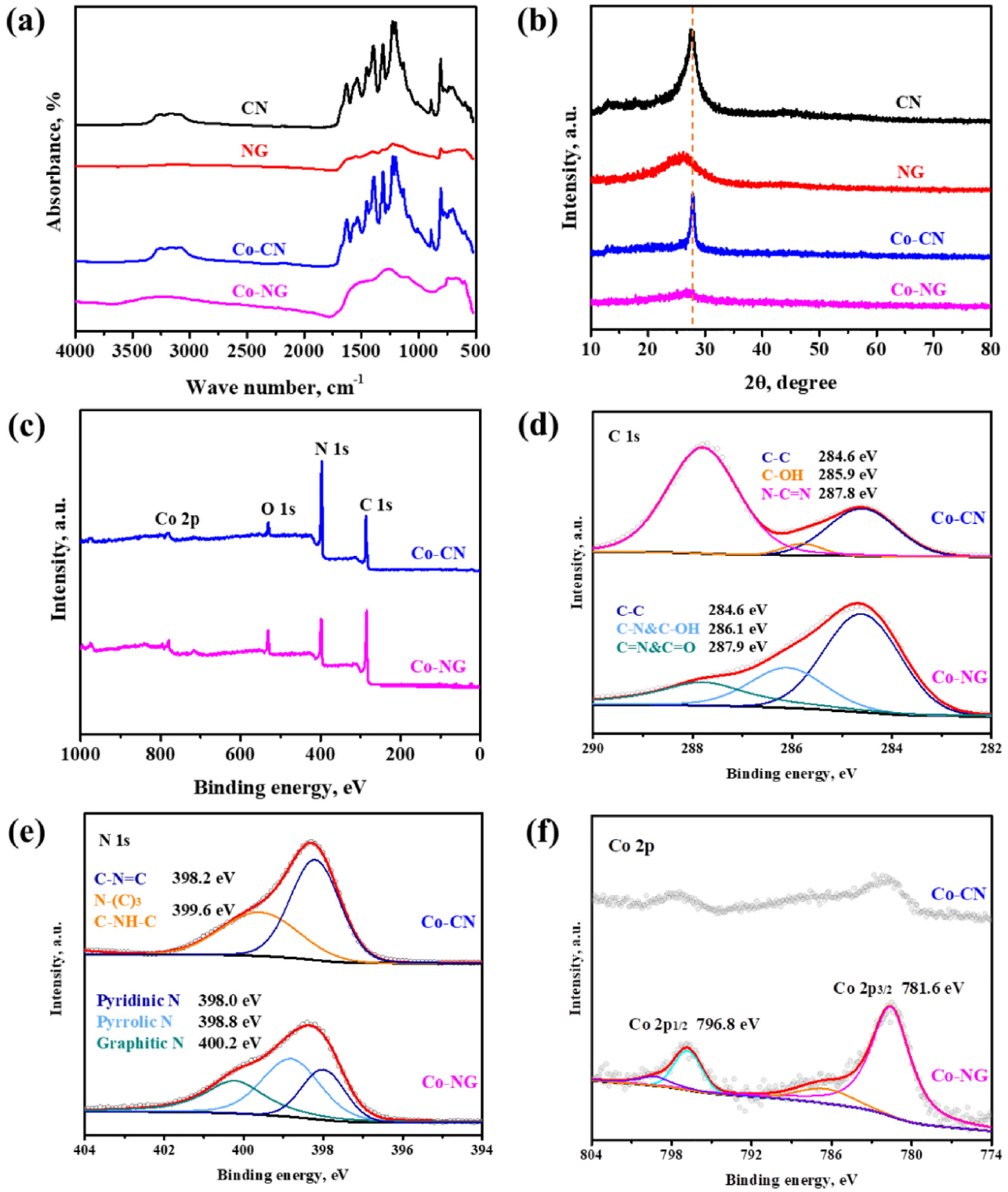

Fig. 2. (a) ATR-FT-IR spectra and (b) XRD patterns of CN, NG, Co-CN, and Co-NG samples. (c) XPS survey spectra of Co-CN and Co-NG samples. Deconvolution of XPS (d) C 1 s, (e) N 1 s, and (f) Co 2p spectra of Co-CN and Co-NG samples.

of DMPOX and for the degradation of BA.

More information could be obtained by evaluating the removal of TOC, shown in Fig. S3. One sees that the value of TOC decreases gradually as the reaction proceeds, and ca. 54% TOC is reduced after 60 min, which is much slower than the rate of BA degradation. These results suggest that there are intermediates during the degradation process before the complete mineralization. The degradation products of BA in the PMS/Co-NG system were analyzed by GC–MS and LC-MS. As shown in Table S1 and S2, low molecular carboxylates such as oxalic acid, malonic acid, and glycerol are observed in the degradation of BA. It is commonly accepted that these intermediates are more resistant to oxidation by $HO^{\bullet}$ and $SO_4^{\bullet-}$ than their aromatics precursor. For instance, the second-order rate constant between $SO_4^{\bullet-}$ and oxalate is only $5.52 \times 10^6\ M^{-1}s^{-1}$ [38], about two orders of magnitude smaller than that between $SO_4^{\bullet-}$ and BA ($1.2 \times 10^9\ M^{-1}s^{-1}$) [36]. As a result, the removal rate of TOC is much slower than that of BA.

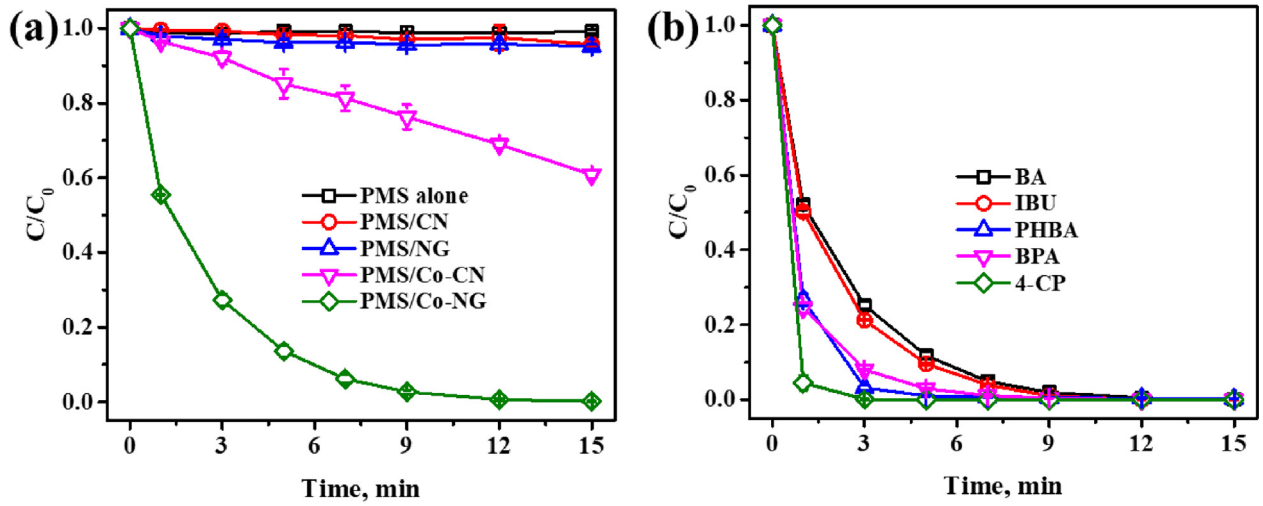

Fig. 3. (a) Degradation of BA by using PMS alone and by using PMS together with different catalysts, and (b) degradation of various organic compounds in PMS/Co-NG system. $[PMS]_0$ = 2.0 mM, $[catalyst]_0$ = 20 mg/L, $[pollutant]_0$ = 50 μM, and pH = 7.0.

3.4. Effect of PMS and Co-NG dosage

The effect of PMS dosage on the removal of BA is shown in Fig. 5a. It can be seen that the degradation of BA in PMS/Co-NG system accelerated as the increase of PMS dosage to 4.0 mM. The inset shows that the initial increase of *k* value is linear in the PMS dosage range from 1.0 mM to 2.0 mM. However, the further increase of *k* value slows down as the PMS dosage is higher than 2.0 mM, possibly due to the quenching effect of excessive PMS towards $SO_4^{\bullet-}$ and $HO^{\bullet}$. Moreover, the degradation rate of BA also increases as the increase of Co-NG dosage from 10 mg/L to 30 mg/L, with *k* value increases from 0.196 min^{-1} to 0.542 min^{-1} (Fig. 5b). The inset shows that the *k* value is linearly proportional to the dosage of Co-NG over a range of 10 mg/L to 30 mg/L. Higher dosage of Co-NG would reasonably provide more accessible active sites, and thus enhance the activation of PMS to produce more $SO_4^{\bullet-}$ and $HO^{\bullet}$ for the degradation of BA.

3.5. Effect of solution chemistry

The effect of solution pH on the degradation of BA in PMS/Co-NG system is shown in Fig. 6a. The degradation rate of BA significantly increases as the increase of solution pH from 4.0 to 7.0, and then decreases as the pH further increases to 10.0. A plot of *k* values vs pH is presented in Fig. S4, exhibiting a bell-shaped profile with a maximum value of 0.390 min^{-1} at pH = 7.0. These results are consistent with previous studies concerning the use of heterogeneous Co-based catalysts for PMS activation [39–41]. The pH-dependent catalytic oxidation performance of PMS/Co-NG could be ascribed to the pH-dependent surface chemical properties of the Co-NG and the species distribution of PMS. It has been reported that the catalytic activity of heterogeneous Co-based catalysts is highly related to the neutral surface hydroxyls (≡Co-OH) [42–44], which are regarded as the most reactive species for the activation of PMS. Normally, most of the surface hydroxyls exist as ≡Co-OH at near neutral condition [42–44]. When pH decreases or increases, protonation or deprotonation reaction occurs, resulting in the reduction of ≡Co-OH. In addition, Fig. S5 shows that Co-NG is negatively charged at pH > 4.0 due to the existence of oxygen-containing functional groups. Consequently, the increase of pH would result in electrostatic repulsion between Co-NG and PMS (pKa_1 less than 0, pKa_2 = 9.4 [45]), and thus slow down the activation of PMS and degradation of BA at high pH = 10.0. Nevertheless, the removal of BA is about 86% and 94% at pH = 5.0 and 9.0, respectively, suggesting the suitability of PMS/Co-NG system over a wide pH range of 5.0–9.0.

The release of Co species during use at different pH conditions was also investigated and shown in Fig. 6b. One sees that the concentration of leached Co decreases from 89.5 to 45.4 μg/L as the pH decreases

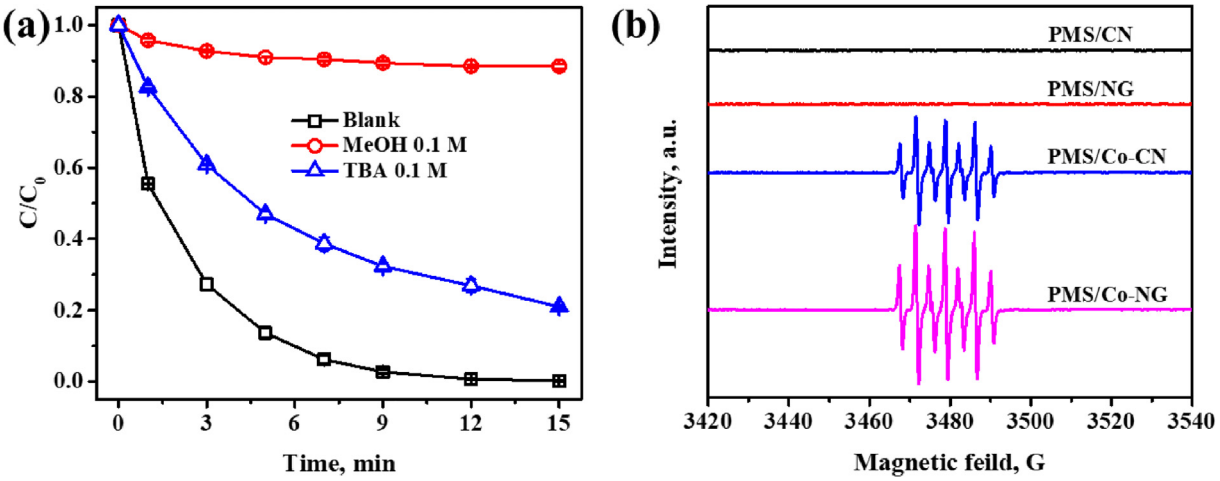

Fig. 4. (a) Effect of radical quenchers on the degradation of BA in PMS/Co-NG system, and (b) EPR spectra of DMPO adducts in different systems. $[PMS]_0$ = 2.0 mM, $[catalyst]_0$ = 20 mg/L, $[BA]_0$ = 50 μM, $[MeOH]_0$ = $[TBA]_0$ = 0.1 M, $[DMPO]_0$ = 100 mM, and pH = 7.0.

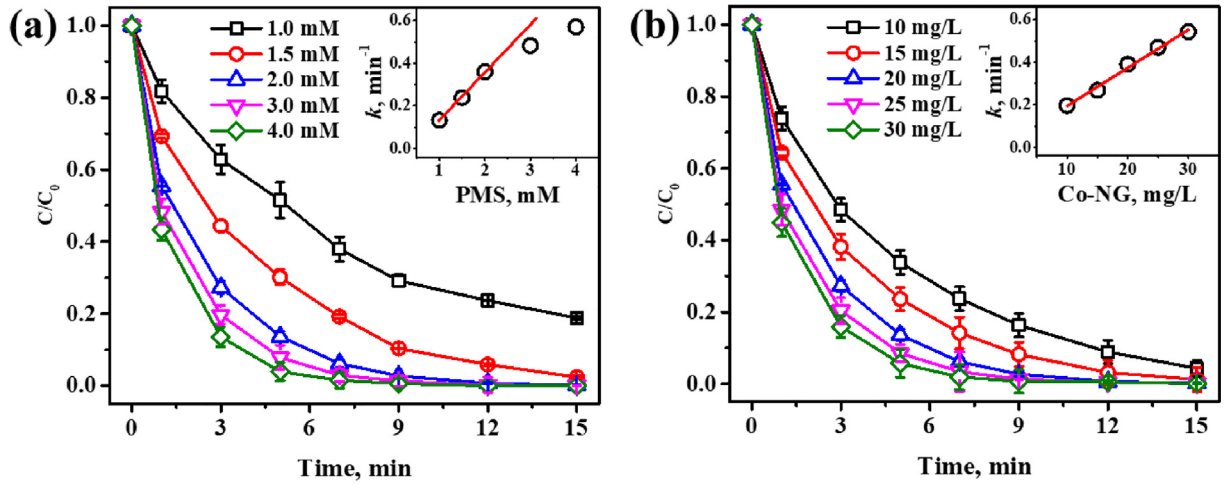

Fig. 5. Effects of (a) PMS and (b) Co-NG dosage on the degradation of BA in PMS/Co-NG system. Insets show the change of the apparent rate constant (k) of BA degradation as a function of PMS or Co-NG dosages. $[BA]_0$ = 50 μM, and pH = 7.0.

from 4.0 to 9.0, and sharply decreases to 1.2 μg/L when pH further increases to 10.0. The leaching of Co could be due to two effects, i.e. the proton effect and the redox of Co(III)/Co(II). In the absence of PMS, the concentration of leached Co form Co-NG is 18.5 and 5.6 μg/L at pH = 4.0 and 5.0, respectively, however, no leached Co is detected at pH > 5.0, suggesting a minor contribution of protons. It is generally accepted that redox reactions of Co(II)/Co(III) are involved in the activation of PMS [7], which would result in a low stability of coordinated Co due to the valence change, and inevitably the leaching of Co. The sharp decrease of Co leaching at pH = 10.0 is probably because of the re-precipitation of Co in the form of Co hydroxide.

It is also important to evaluate the effects of inorganic anions and NOM that are ubiquitous in native water on the catalytic reactions. For example, the typical concentration of Cl^-, HCO_3^- is usually in a range of tens to hundreds of mg/L, and the level of NOM could reach tens of mgC/L in natural water bodies [46]. Fig. 7a shows the impact of Cl^-, SO_4^{2-}, NO_3^-, and HCO_3^- on the degradation of BA in the PMS/Co-NG system. Both SO_4^{2-} and NO_3^- exhibit negligible influence on the degradation of BA, while only 88% and 63% of BA is removed in the presence of 10 mM Cl^- and HCO_3^-, respectively. The hypothesis is that both Cl^- and HCO_3^- could consume $SO_4^{\bullet-}$ and $HO^\bullet$ by reacting to form less oxidative chlorine radicals (i.e., $HOCl^{\bullet-}$, and $Cl^\bullet$) and carbonate radicals ($CO_3^{\bullet-}$), respectively (eqs. 2–6) [47–51]. The effect of NOM on the degradation of BA is shown in Fig. 7b, from which one sees that NOM significantly retards the degradation of BA in PMS/Co-NG system. The more NOM (up to 20 mgC/L) is present, the stronger inhibition is observed. These results are not surprising as NOM could act as a radical scavenger for both $SO_4^{\bullet-}$ and $HO^\bullet$ with second-order rate constant of 6.8×10^3 $mgC^{-1}s^{-1}$ and 1.4×10^4 $mgC^{-1}s^{-1}$, respectively [51–53], and thus inhibit the degradation of BA due to the competition of the reactive species.

$SO_4^{\bullet-} + Cl^- \rightarrow SO_4^{2-} + Cl^\bullet$ $k = 3.0 \times 10^8$ $M^{-1}s^{-1}$ (2)

$HO^\bullet + Cl^- \leftrightarrow HOCl^{\bullet-} + HO^-$ $k_f = 4.3 \times 10^9$ $M^{-1}s^{-1}$, $k_r = 6.1 \times 10^9$ $M^{-1}s^{-1}$ (3)

$HOCl^{\bullet-} + H^+ \leftrightarrow Cl^\bullet + H_2O$ $k_f = 2.6 \times 10^{10}$ $M^{-1}s^{-1}$, $k_r = 3.6 \times 10^3$ $M^{-1}s^{-1}$ (4)

$SO_4^{\bullet-} + HCO_3^- \rightarrow CO_3^{\bullet-} + SO_4^{2-} + H^+$ $k = 3.5 \times 10^6$ $M^{-1}s^{-1}$ (5)

$HO^\bullet + HCO_3^- \rightarrow CO_3^{\bullet-} + H_2O$ $k = 8.5 \times 10^6$ $M^{-1}s^{-1}$ (6)

3.6. Reusability

Reusability is a crucial factor that greatly determines the suitability of the heterogeneous catalysts in real application. The reusability of Co-NG was investigated by five consecutive degradation experiments. Results in Fig. 7c show that nearly 100% BA is degraded in each run of

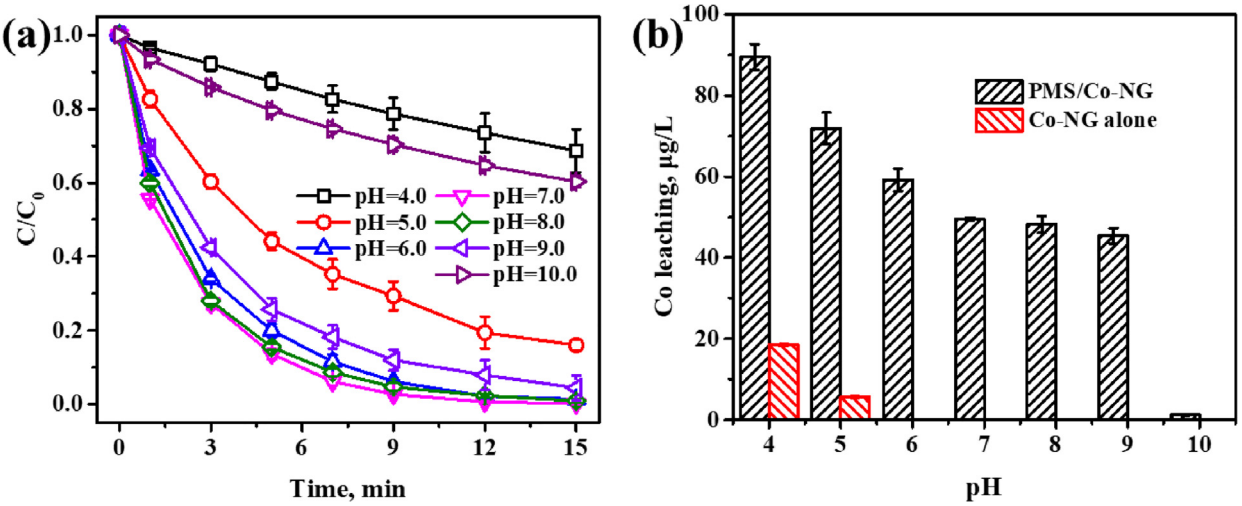

Fig. 6. (a) Effect of solution pH on the degradation of BA and (b) the corresponding Co leaching in PMS/Co-NG system. $[PMS]_0$ = 2.0 mM, $[Co\text{-}NG]_0$ = 20 mg/L, $[BA]_0$ = 50 μM.

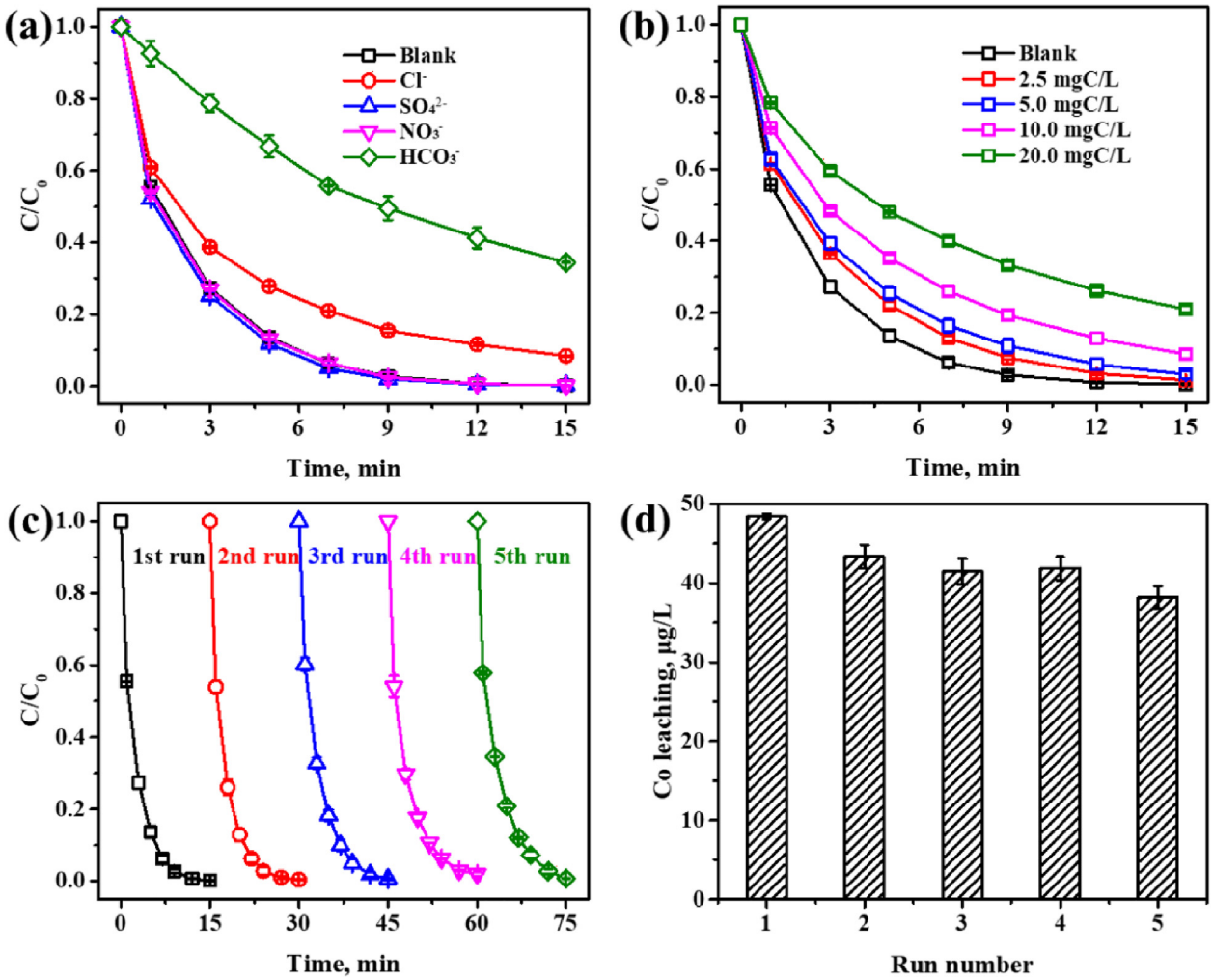

Fig. 7. Effects of (a) inorganic anions (10 mM) and (b) NOM on the degradation of BA in PMS/Co-NG system. The (c) BA degradation and (d) Co leaching in five consecutive experiments of the Co-NG catalyst. $[PMS]_0$ = 2.0 mM, $[Co\text{-}NG]_0$ = 20 mg/L, $[BA]_0$ = 50 μM, and pH = 7.0.

15 min, while the *k* value gradually decreases from 0.39 to 0.28 min^{-1} as the increase of the cycle number to five times (Table S3). The decrease of *k* value is contributed to the leaching of Co, as its concentration in solution decreases gradually from 49.6 μg/L (3.1 wt% in Co-NG) to 38.2 μg/L (2.4 wt% in Co-NG) (Fig. 7d). However, the leached Co in PMS/Co-NG process is much less than of Co oxides mediated PMS activation processes [54], demonstrating a good reusability and stability of the Co-NG catalyst for the activation of PMS and for the degradation of organic pollutants in water.

4. Conclusions

In this study, we report the preparation of a Co-NG sample with high Co content of 8.0 wt%, essentially dispersed Co atoms coordinated by N atoms in carbonaceous substrate, through a heating treatment of Co phthalocyanine and melamine. The sample demonstrated superior catalytic activity for the activation of PMS for the degradation of organic contaminations, due to the its high specific surface area as well as the high Co content. Both $SO_4^{\bullet -}$ and $HO^{\bullet}$ are involved in the PMS/Co-NG system, in which $SO_4^{\bullet -}$ is identified as the main reactive species for the degradation of BA. The PMS/Co-NG system could degrade BA over a wide pH range of 5.0 to 9.0 and in the presence of inorganic anions and NOM. The degradation of BA could be improved by using larger dosage of PMS and Co-NG. In addition, the strong binding affinity between Co atoms and N atoms renders Co-NG with good stability and reusability, showing leached Co in solution less than 50 μg/L for each run at neutral condition. We hope our study provides an easy strategy for highly efficient and robust Co-based catalysts for environmental remediation.

Declaration of Competing Interest

The authors declare that they have no known competing financial interests or personal relationships that could have appeared to influence the work reported in this paper.

Acknowledgments

The authors thank the financial support from Natural Science Foundation of China (51573079 and 21925602), and the Fundamental Research Funds for the Central Universities (30920021116)

Appendix A. Supplementary data

Supplementary data to this article can be found online at https://doi.org/10.1016/j.cej.2020.126395.

References

[1] J. Lee, U. von Gunten, J.H. Kim, Persulfate-based advanced oxidation: Critical assessment of opportunities and roadblocks, Environ. Sci. Technol. 54 (2020) 3064–3081.
[2] Y. Lei, J. Lu, M. Zhu, J. Xie, S. Peng, C. Zhu, Radical chemistry of diethyl phthalate

oxidation via UV/peroxymonosulfate process: Roles of primary and secondary radicals, Chem. Eng. J. 379 (2020) 122339.
[3] R. Yin, W. Guo, H. Wang, J. Du, X. Zhou, Q. Wu, H. Zheng, J. Chang, N. Ren, Enhanced peroxymonosulfate activation for sulfamethazine degradation by ultrasound irradiation: Performances and mechanisms, Chem. Eng. J. 335 (2018) 145–153.
[4] C. Qi, X. Liu, C. Lin, H. Zhang, X. Li, J. Ma, Activation of peroxymonosulfate by microwave irradiation for degradation of organic contaminants, Chem. Eng. J. 315 (2017) 201–209.
[5] Z. Liu, H. Ding, C. Zhao, T. Wang, P. Wang, D.D. Dionysiou, Electrochemical activation of peroxymonosulfate with ACF cathode: Kinetics, influencing factors, mechanism, and application potential, Water Res. 159 (2019) 111–121.
[6] S. Zhou, Y. Yu, W. Zhang, X. Meng, J. Luo, L. Deng, Z. Shi, J. Crittenden, Oxidation of microcystin-LR via activation of peroxymonosulfate using ascorbic acid: Kinetic modeling and toxicity assessment, Environ. Sci. Technol. 52 (2018) 4305–4312.
[7] G.P. Anipsitakis, D.D. Dionysiou, Radical generation by the interaction of transition metals with common oxidants, Environ. Sci. Technol. 38 (2004) 3705–3712.
[8] Y. Ding, W. Nie, W. Li, Q. Chang, Co-doped $NaBiO_3$ nanosheets with surface confined Co species: High catalytic activation of peroxymonosulfate and ultra-low Co leaching, Chem. Eng. J. 356 (2019) 359–370.
[9] Z. Li, M. Wang, C. Jin, J. Kang, J. Liu, H. Yang, Y. Zhang, Q. Pu, Y. Zhao, M. You, Synthesis of novel Co_3O_4 hierarchical porous nanosheets via corn stem and MOF-Co templates for efficient oxytetracycline degradation by peroxymonosulfate activation, Chem. Eng. J. 392 (2019) 123789.
[10] Z. Chen, L. Wang, H. Xu, Q. Wen, Efficient heterogeneous activation of peroxymonosulfate by modified $CuFe_2O_4$ for degradation of tetrabromobisphenol A, Chem. Eng. J. 389 (2020) 124345.
[11] J. Lim, M.R. Hoffmann, Peroxymonosulfate (PMS) activation on cobalt-doped TiO_2 nanotubes: degradation of organics under dark and solar light irradiation conditions, Environ. Sci.: Nano (2020).
[12] J. Lim, Y. Yang, M.R. Hoffmann, Activation of peroxymonosulfate by oxygen vacancies-enriched cobalt-doped black TiO_2 nanotubes for the removal of organic pollutants, Environ. Sci. Technol. 53 (2019) 6972–6980.
[13] J.C. Espinosa, P. Manickam-Periyaraman, F. Bernat-Quesada, S. Sivanesan, M. Álvaro, H. García, S. Navalón, Engineering of activated carbon surface to enhance the catalytic activity of supported cobalt oxide nanoparticles in peroxymonosulfate activation, Appl. Catal. B Environ. 249 (2019) 42–53.
[14] H. Xu, N. Jiang, D. Wang, L. Wang, Y. Song, Z. Chen, J. Ma, T. Zhang, Improving PMS oxidation of organic pollutants by single cobalt atom catalyst through hybrid radical and non-radical pathways, Appl. Catal. B Environ. 263 (2020) 118350.
[15] W. Du, Q. Zhang, Y. Shang, W. Wang, Q. Li, Q. Yue, B. Gao, X. Xu, Sulfate saturated biosorbent-derived Co-S@NC nanoarchitecture as an efficient catalyst for peroxymonosulfate activation, Appl. Catal. B Environ. 262 (2020) 118302.
[16] H. Li, C. Shan, B. Pan, Fe(III)-doped g-C_3N_4 mediated peroxymonosulfate activation for selective degradation of phenolic compounds via high-valent iron-oxo species, Environ. Sci. Technol. 52 (2018) 2197–2205.
[17] H. Li, C. Shan, B. Pan, Development of Fe-doped g-C_3N_4/graphite mediated peroxymonosulfate activation for degradation of aromatic pollutants via nonradical pathway, Sci. Total Environ. 675 (2019) 62–72.
[18] S. An, G. Zhang, T. Wang, W. Zhang, K. Li, C. Song, J.T. Miller, S. Miao, J. Wang, X. Guo, High-density ultra-small clusters and single-atom Fe sites embedded in graphitic carbon nitride (g-C_3N_4) for highly efficient catalytic advanced oxidation processes, ACS Nano 12 (2018) 9441–9450.
[19] L. Wang, X. Guo, Y. Chen, S. Ai, H. Ding, Cobalt-doped g-C_3N_4 as a heterogeneous catalyst for photo-assisted activation of peroxymonosulfate for the degradation of organic contaminants, Appl. Surf. Sci. 467–468 (2019) 954–962.
[20] M. Xie, J. Tang, L. Kong, W. Lu, V. Natarajan, F. Zhu, J. Zhan, Cobalt doped g-C_3N_4 activation of peroxymonosulfate for monochlorophenols degradation, Chem. Eng. J. 360 (2019) 1213–1222.
[21] J. Ma, Q. Yang, Y. Wen, W. Liu, Fe-g-C_3N_4/graphitized mesoporous carbon composite as an effective Fenton-like catalyst in a wide pH range, Appl. Catal. B Environ. 201 (2017) 232–240.
[22] Q. Liu, Y. Guo, Z. Chen, Z. Zhang, X. Fang, Constructing a novel ternary Fe(III)/graphene/g-C_3N_4 composite photocatalyst with enhanced visible-light driven photocatalytic activity via interfacial charge transfer effect, Appl. Catal. B Environ. 183 (2016) 231–241.
[23] Y. Liu, Y. Fan, Z. Liu, Pyrolysis of iron phthalocyanine on activated carbon as highly efficient non-noble metal oxygen reduction catalyst in microbial fuel cells, Chem. Eng. J. 361 (2019) 416–427.
[24] H. Wu, H. Li, X. Zhao, Q. Liu, J. Wang, J. Xiao, S. Xie, R. Si, F. Yang, S. Miao, X. Guo, G. Wang, X. Bao, Highly doped and exposed Cu(I)-N active sites within graphene towards efficient oxygen reduction for zinc-air batteries, Energy Environ. Sci. 9 (2016) 3736–3745.
[25] P. Chen, K. Li, Y. Yu, W. Zhang, Cobalt-doped graphitic carbon nitride photocatalysts with high activity for hydrogen evolution, Appl. Surf. Sci. 392 (2017) 608–615.
[26] H. Li, C. Shan, W. Li, B. Pan, Peroxymonosulfate activation by iron(III)-tetraamidomacrocyclic ligand for degradation of organic pollutants via high-valent iron-oxo complex, Water Res. 147 (2018) 233–241.
[27] G. Lalande, G. Faubert, R. Cote, D. Guay, J.P. Dodelet, L.T. Weng, P. Bertrand, Catalytic activity and stability of heat-treated iron phthalocyanines for the electroreduction of oxygen in polymer electrolyte fuel cells, J. Power Sources 61 (1996) 227–237.
[28] X. Wu, H. Ma, W. Zhong, J. Fan, H. Yu, Porous crystalline g-C_3N_4: Bifunctional $NaHCO_3$ template-mediated synthesis and improved photocatalytic H_2-evolution rate, Appl. Catal. B Environ. 271 (2020) 118899.
[29] Q. Gao, J. Xu, Z. Wang, Y. Zhu, Enhanced visible photocatalytic oxidation activity of perylene diimide/g-C_3N_4 n-n heterojunction via π-π interaction and interfacial charge separation, Appl. Catal. B Environ. 271 (2020) 118933.
[30] J. Huang, D. Li, R. Li, Q. Zhang, T. Chen, H. Liu, Y. Liu, W. Lv, G. Liu, An efficient metal-free phosphorus and oxygen co-doped g-C_3N_4 photocatalyst with enhanced visible light photocatalytic activity for the degradation of fluoroquinolone antibiotics, Chem. Eng. J. 374 (2019) 242–253.
[31] F. Pan, Z. Cao, Q. Zhao, H. Liang, J. Zhang, Nitrogen-doped porous carbon nanosheets made from biomass as highly active electrocatalyst for oxygen reduction reaction, J. Power Sources 272 (2014) 8–15.
[32] M. Zhu, J. Chen, R. Guo, J. Xu, X. Fang, Y. Han, Cobalt phthalocyanine coordinated to pyridine-functionalized carbon nanotubes with enhanced CO_2 electroreduction, Appl. Catal. B Environ. 251 (2019) 112–118.
[33] J. Hou, J. Lin, H. Fu, Y. Wan, X. Qu, Z. Xu, S. Zheng, Vitamin B_{12} derived CoCNx composite confined in SBA-15 as highly effective catalyst to activate peroxymonosulfate for naproxen degradation, Chem. Eng. J. 389 (2020) 124344.
[34] X. Duan, C. Su, J. Miao, Y. Zhong, Z. Shao, S. Wang, H. Sun, Insights into perovskite-catalyzed peroxymonosulfate activation: Maneuverable cobalt sites for promoted evolution of sulfate radicals, Appl. Catal. B Environ. 220 (2018) 626–634.
[35] G.V. Buxton, C.L. Greenstock, W.P. Helman, A.B. Ross, Critical review of rate constants for reactions of hydrated electrons, hydrogen atoms and hydroxyl radicals ($\cdot OH/O^{\cdot-}$) in aqueous solution, J. Phys. Chem. Ref. Data 17 (1988) 513–886.
[36] P. Neta, R.E. Huie, A.B. Ross, Rate constants for reactions of inorganic radicals in aqueous solution, J. Phys. Chem. Ref. Data 17 (1988) 1027–1284.
[37] X. Yang, J. Cai, X. Wang, Y. Li, Z. Wu, W.D. Wu, X.D. Chen, J. Sun, S. Sun, Z. Wang, A bimetallic Fe–Mn oxide-activated oxone for in situ chemical oxidation (ISCO) of trichloroethylene in groundwater: Efficiency, sustained activity, and mechanism investigation, Environ. Sci. Technol. 54 (2020) 3714–3724.
[38] R.E. Huie, C.L. Clifton, Kinetics of the reaction of the sulfate radical with the oxalate anion, Int. J. Chem. Kinet. 28 (1996) 195–199.
[39] S. Wang, J. Wang, Peroxymonosulfate activation by Co_9S_8@ S and N co-doped biochar for sulfamethoxazole degradation, Chem. Eng. J. 385 (2020) 123933.
[40] M. Wu, K. Fu, H. Deng, J. Shi, Cobalt tetracarboxyl phthalocyanine-manganese octahedral molecular sieve (OMS-2) as a heterogeneous catalyst of peroxymonosulfate for degradation of diclofenac, Chemosphere 219 (2019) 756–765.
[41] J. Zhu, J. Wang, C. Shan, J. Zhang, L. Lv, B. Pan, Durable activation of peroxymonosulfate mediated by Co-doped mesoporous $FePO_4$ via charge redistribution for atrazine degradation, Chem. Eng. J. 375 (2019) 122009.
[42] Y. Ren, L. Lin, J. Ma, J. Yang, J. Feng, Z. Fan, Sulfate radicals induced from peroxymonosulfate by magnetic ferrospinel MFe_2O_4 (M = Co, Cu, Mn, and Zn) as heterogeneous catalysts in the water, Appl. Catal. B Environ. 165 (2015) 572–578.
[43] H. Zhang, C. Li, L. Lyu, C. Hu, Surface oxygen vacancy inducing peroxymonosulfate activation through electron donation of pollutants over cobalt-zinc ferrite for water purification, Appl. Catal. B Environ. 270 (2020) 118874.
[44] Y. Wang, Z. Chi, C. Chen, C. Su, D. Liu, Y. Liu, X. Duan, S. Wang, Facet- and defect-dependent activity of perovskites in catalytic evolution of sulfate radicals, Appl. Catal. B Environ. 272 (2020) 118972.
[45] Y. Rao, F. Han, Q. Chen, D. Wang, D. Xue, H. Wang, S. Pu, Efficient degradation of diclofenac by $LaFeO_3$-catalyzed peroxymonosulfate oxidation-kinetics and toxicity assessment, Chemosphere 218 (2019) 299–307.
[46] J.D. Hem, Study and interpretation of the chemical characteristics of natural water, 3rd ed. ed., Reston, VA, 1985.
[47] L. Hu, G. Zhang, M. Liu, Q. Wang, P. Wang, Enhanced degradation of Bisphenol A (BPA) by peroxymonosulfate with Co_3O_4-Bi_2O_3 catalyst activation: Effects of pH, inorganic anions, and water matrix, Chem. Eng. J. 338 (2018) 300–310.
[48] J. Li, M. Xu, G. Yao, B. Lai, Enhancement of the degradation of atrazine through $CoFe_2O_4$ activated peroxymonosulfate (PMS) process: Kinetic, degradation intermediates, and toxicity evaluation, Chem. Eng. J. 348 (2018) 1012–1024.
[49] L. Wang, J. Jiang, S. Pang, Y. Zhou, J. Li, S. Sun, Y. Gao, C. Jiang, Oxidation of bisphenol A by nonradical activation of peroxymonosulfate in the presence of amorphous manganese dioxide, Chem. Eng. J. 352 (2018) 1004–1013.
[50] Y. Xu, Z. Lin, Y. Wang, H. Zhang, The UV/peroxymonosulfate process for the mineralization of artificial sweetener sucralose, Chem. Eng. J. 317 (2017) 561–569.
[51] P. Hu, M. Long, Cobalt-catalyzed sulfate radical-based advanced oxidation: A review on heterogeneous catalysts and applications, Appl. Catal. B Environ. 181 (2016) 103–117.
[52] S. Khan, X. He, J.A. Khan, H.M. Khan, D.L. Boccelli, D.D. Dionysiou, Kinetics and mechanism of sulfate radical- and hydroxyl radical-induced degradation of highly chlorinated pesticide lindane in UV/peroxymonosulfate system, Chem. Eng. J. 318 (2017) 135–142.
[53] Y. Feng, Q. Song, W. Lv, G. Liu, Degradation of ketoprofen by sulfate radical-based advanced oxidation processes: Kinetics, mechanisms, and effects of natural water matrices, Chemosphere 189 (2017) 643–651.
[54] G.P. Anipsitakis, E. Stathatos, D.D. Dionysiou, Heterogeneous activation of oxone using Co_3O_4, J. Phys. Chem. B 109 (2005) 13052–13055.